Cosmic web alignments with the shape, angular momentum and peculiar velocities of dark matter halos

Jaime E. Forero-Romero[1], Sergio Contreras[2], Nelson Padilla[2]

[1] *Uni A* [2] *Uni B*

10 February 2014

ABSTRACT

We study the alignment of DM halos with the cosmic web as described by the tidal and velocity shear fields. We focus on the alignment of halos shape, spin and peculiar velocities. We use a cosmological N-body simulation that allows to study dark matter halos spanning four orders of magnitude in mass $((10^{10}$-$10^{14})$ $h^{-1}\mathrm{M}_\odot$ and spatial scales of $(0.5$-$1.0)h^{-1}\mathrm{Mpc}$ to define the cosmic web. After varying the numerical parameters in our experiments we find that the tidal field provides a robust description for the different kinds of alignments. We measure a strong here is a strong alignment of the peculiar velocity field and the halo shape with the cosmic web defined by the tidal field. The results for the spin alignment are less significant. The shape alignment is stronger for halos that are either massive ($M > 10^{12}h^{-1}\mathrm{M}_\odot$), have large or are located in high density regions.

Key words: methods: N-body simulations, galaxies: haloes, cosmology: theory, dark matter, large-scale structure of Universe

1 INTRODUCTION

The formation of large scale structure in the Universe proceeds by gravitational instability. This is an intrinsic anisotropic process. [Pancake formation ...]

Numerical simulations allow the exploration of a deep nonlinear regime, following the formation of virialized dark matter halos, which host observable galaxies. Some characteristics of these halos have to be linked to the environment in which they formed. One way to studty the connection halo-environment is to quantify the degree of correlation between different halo properties and their surrounding density and velocity fields.

Among the properties that are of interest we find the shape, spin and peculiar velocity. [Relevanc of dark matter halo shapes ...] [Relevance of halo spin ...] [Relevance of peculiar velocities]

There is large tradition of theoretical precedents for the measurements of shape and spin alignment. In this paper we review most of these studyes and offer our own study with complementary numerical techniques and simulations. [Brief summary of the appendix ...]

We also present the results for the alignment of peculiar velocities with large scale structure. Such a study has received less atention in the literature. However, we consider that it presents relevant insights for the study of cosmic flows.

The structure of this paper is the following. In §2 we present the theoretical antecedendts for the alignment studies we present in this paper. In §3 we present the N-body cosmological simulation and halo catalogs next to describe in §4 the two web-finding algorithms we use. In §6 we present our main results about the alignment of shape, spin and peculiar velocities with respect to the cosmic web. We continue with a discussion of these results in §7 paying special attention to resolution effects and the conditions that might drive the strong alignment signals observed in the precedent section. In §8 we present our conclusions.

2 THEORETICAL CONSIDERATIONS: NOTATION AND PRECEDENTS

There is abundant literature on the issue of shape and angular momentum aligmnent of dark matter haloe with respect to the cosmic web. In this paper we focus our attention on results published during the last decade that have made use of large N-body dark matter only cosmological simulations. There are many works that have addressed this problem using observational data from large surveys such as the Sloan Digital Sky Survey (SDSS), however we choose to narrow our discussion to simulation based studies which are prone to comparison.

Out of the three alignments that we study in this paper -shape, angular momentum and peculiar velocity- only the the first two have received wide attention in the literature,

Author	Web Method	Halo Finder	Major Axis	Correlation
SHAPE				

being angular momentum the most popular with twice the number of studies for shape alignment.

These alignments are often measured from the distribution of the $\mu = |\cos\theta|$ where θ is the angle between the two axes of interest. This is often directly measuered as the absolute value of the dot product between the two unit vectors along the directions being tested, for instance in the case of angular momentum one would compute $\mu = |\hat{j} \cdot \hat{n}|$ In the case of shape alignments the major axis is the chosen direction to compare against the cosmic web.

For an isotropic ditribution of the vector around the direction defined by $\hat{n}$ the μ distribution, ranging between 0 and 1, should be flat and its mean value shoud be $\langle |mu| \rangle = 0.5$. If a distribution is biased towards 1 ($\langle |\mu| \rangle > 0.5$) we call this an statistical alignment along $\hat{n}$, while in the case of a bias towards 0 ($\langle |\mu| \rangle < 0.5$) we talk about an anti-alignment, meaning an perpendicular orientations with respecto to the $\hat{n}$ direction.

a Trowland et al. (2013) presented a parameterization for the μ distribution in the case of angular momentm alignment based on theoretical considerations by Lee et al. (2005) (Eq. 6 in the Appendix A). Under this parameterization it was found a unique correspondece between the full shape of the $|\mu|$ distribution and its average. In this paper we use that result to only present the results for the average $\langle |\mu| \rangle$.

Table 1 and Table 2 summarize recent results found in the literature for shape and angular momentum alignment. The Appendix A includes a detailed description of the definitions, algorithms and simulations used in each one of these studies. In these tables the first column describe the reference, the second column summarizes the web finding method with a single name, the third scale associates an spatial scale to the web finding methods, in most cases it corresponds to the grid size or smoothing scale used to interpolate the underlying matter density or velocity field; The fourth column indicates along which web element (filament or wall) was measured the alignment; the fifth colume indicates the strenght of the alignment/anti-alignment, $++/--$ indicate a strong alignement/anti-alignment while $+/-$ indicate a weaker signal; the last columns indicates whether the described signal is present within a defined range of halo mass.

These results can be summarized in three important points:

• The halo mass of $1 - 5 \times 10^{12} h^{-1} M_\odot$ is a threshold mass between behaviours of no-alignment, alignment or anti-alignment.
• Halo shape provides a strong alignment signal along filaments and sheets, more so for massive haloes.
• Halo spin tends to be oriented perpendicular to filaments and parallel to sheets, but it is a weaker than shape alignment.

3 N-BODY SIMULATION AND HALO FINDING

In this paper we use the Bolshoi simulation that follows the non-linear evolution of a dark matter density field on cosmo-

logical scales. The volume is a cubic box with $250h^{-1}$Mpc on a side, the matter density field is sampled with 2048^3 particles. The cosmological parameters in the simulation correspond to the results inferred from WMAP5 data (Dunkley et al. 2009), which are also consistent with the more recent results of WMAP9 (Hinshaw et al. 2013). These parameters are $\Omega_m = 0.27$, $\Omega_\Lambda = 0.73$, $\sigma_8 = 0.82$, $n_s = 0.95$ and $h = 0.70$ for the matter density, cosmological constant, normalization of the power spectrum, the slope in the spectrum of the primordial matter fluctuation and the dimensionless Hubble constant. With this conditions the mass of each dark matter particle in the simulation corresponds to $m_p = 1.4 \times 10^8 h^{-1} M_\odot$. A more detailed description of the simulation can be found in (Klypin et al. 2011).

In this paper we use groups found with a Friends-Of-Friends (FOF) halo finder using a linking length of $b = 0.17$ times the mean interparticle separation. This choice translates into halos with a density of 570 times the mean density at $z = 0$. The measurements for the shape, angular momentum and peculiar velocity are done using the set of particles in each dark matter halo. The definition we use in this paper for the shape comes from the diagonalization of the reduced inertia tensor.

$$\mathcal{T}_{lm} = \sum_i \frac{x_{i,l} x_{i,m}}{R_i^2}, \tag{1}$$

where i is the particle index in the halo and l, m run over the three spatial indexes and $R_i^2 = x_{i,1}^2 + x_{i,2}^2 + x_{i,3}^2$, where the positions are measured with respect to the center of mass.

The spin is calculated as

$$\vec{J} = \sum_i m_p R_i \vec{v}_i, \tag{2}$$

where the velocities are also measured with respect to the center of mass velocity. Finally the peculiar velocity of a halo is computed as the center of mass velocity.

The halo data used in this paper is publicly available through the MultiDark database[1] and is thoroughly described in Riebe et al. (2013).

4 WEB FINDING ALGORITHMS

We use two algorithms to define the cosmic web in cosmological N-body simulations. Both are based on the same algorithmic principle, which determines locally a symmetric tensor which can be diagonalized to yield three real eigenvalues $\lambda_1 > \lambda_2 > \lambda_3$ and their corresponding eigenvectors $\mathbf{e}_1$, $\mathbf{e}_2$ and $\mathbf{e}_3$. This allows for a local classification into one of the following four web types: void, sheet, filament and peak depending on the number of eigenvalues larger than a given threshold λ_{th} is 3, 2, 1 or 0, respectively.

We use two different symmetric tensors. The first is the shear tensor, defined as the Hessian of the gravitational potential, normalized in such a way as to be dimensionless:

$$T_{\alpha\beta} = \frac{\partial^2 \phi}{\partial r_\alpha \partial r_\beta}, \tag{3}$$

---

[1] http://www.multidark.org/MultiDark/

Author	Web Method	Spatial Scale	Along	Alignment	Mass dependence
Forero-Romero et al. (2014)	T-Web	$0.5 - 1h^{-1}\mathrm{Mpc}$	filament	++	$> 10^{12}h^{-1}\mathrm{M}_\odot$
			filament	+	$< 10^{12}h^{-1}\mathrm{M}_\odot$
			wall	++	$> 10^{12}h^{-1}\mathrm{M}_\odot$
			wall	+	$< 10^{12}h^{-1}\mathrm{M}_\odot$
Forero-Romero et al. (2014)	Vp-Web	$0.5 - 1h^{-1}\mathrm{Mpc}$	filament	$--$	$> 10^{12}h^{-1}\mathrm{M}_\odot$
			filament	none	$< 10^{12}h^{-1}\mathrm{M}_\odot$
			wall	$--$	$> 10^{12}h^{-1}\mathrm{M}_\odot$
			wall	none	$< 10^{12}h^{-1}\mathrm{M}_\odot$
Libeskind et al. (2013)	V-Web	$1h^{-1}\mathrm{Mpc}$	filament	++	$> 10^{12}h^{-1}\mathrm{M}_\odot$
			filament	+	$< 10^{12}h^{-1}\mathrm{M}_\odot$
			wall	++	all masses
Zhang et al. (2009)	Hessian density field	$2.1h^{-1}\mathrm{Mpc}$	filament	++	$> 10^{12}h^{-1}\mathrm{M}_\odot$
			filament	+	$< 10^{12}h^{-1}\mathrm{M}_\odot$
Aragón-Calvo et al. (2007)	Hessian density field	-	wall	++	$> 10^{12}h^{-1}\mathrm{M}_\odot$
		-	wall	+	$< 10^{12}h^{-1}\mathrm{M}_\odot$
		-	filament	++	$> 10^{12}h^{-1}\mathrm{M}_\odot$
		-	filament	+	$< 10^{12}h^{-1}\mathrm{M}_\odot$

Table 1. Shape alignment with the cosmic web. Summary of theoretical results provided by methods similar to ours.

Author	Web Method	Spatial Scale $(h^{-1}\mathrm{Mpc})$	Along	Alignment	Mass dependence
Forero-Romero et al. (2014)	T-Web	$0.5 - 1$	filament	none	$< 10^{12}h^{-1}\mathrm{M}_\odot$
			filament	-	$> 10^{12}h^{-1}\mathrm{M}_\odot$
			wall	none	$< 10^{12}h^{-1}\mathrm{M}_\odot$
			wall	none	$> 10^{12}h^{-1}\mathrm{M}_\odot$
Forero-Romero et al. (2014)	Vp-Web	$0.5 - 1$	filament	none	$< 10^{12}h^{-1}\mathrm{M}_\odot$
			filament	none	$> 10^{12}h^{-1}\mathrm{M}_\odot$
			wall	none	$< 10^{12}h^{-1}\mathrm{M}_\odot$
			wall	+	$> 10^{12}h^{-1}\mathrm{M}_\odot$
Libeskind et al. (2013)	V-Web	1	filament	$-$	$> 10^{12}h^{-1}\mathrm{M}_\odot$
			filament	+	$< 10^{12}h^{-1}\mathrm{M}_\odot$
			wall	++	all masses
Trowland et al. (2013)	Hessian density	$2 - 5$	filament	$-$	$> 5 \times 10^{12}h^{-1}\mathrm{M}_\odot$
			filament	+	$< 5 \times 10^{12}h^{-1}\mathrm{M}_\odot$
Codis et al. (2012)	Morse Theory & T-Web	$1 - 5$	filament	$--$	$> 10^{12.5}h^{-1}\mathrm{M}_\odot$
			filament	++	$< 10^{12.5}h^{-1}\mathrm{M}_\odot$
			wall	++	all masses
Zhang et al. (2009)	Hessian density	2.1	filament	++	if anticorrelated with shape
			filament	$--$	if correlated with shape
Aragón-Calvo et al. (2007)	Hessian density	-	wall	++	$> 10^{12}h^{-1}\mathrm{M}_\odot$
		-	wall	+	$< 10^{12}h^{-1}\mathrm{M}_\odot$
		-	filament	$-$	$> 10^{12}h^{-1}\mathrm{M}_\odot$
		-	filament	+	$< 10^{12}h^{-1}\mathrm{M}_\odot$
Hahn et al. (2007)	Tidal Web	2.1	filament	$-$	none
			wall	+	$< 10^{12}h^{-1}\mathrm{M}_\odot$
			wall	++	$> 10^{12}h^{-1}\mathrm{M}_\odot$

Table 2. Spin alignment with the cosmic web. Summary of theoretical results provided by methods similar to ours.

where ϕ is the gravitational potential rescaled by a factor $4\pi G\bar{\rho} = 3/2\Omega_m H_0^2$ in such a way that the Poission equation can be written as $\nabla^2\phi = \delta$, where δ is the matter over-density, $\bar{\rho}$ is the average matter density, H_0 is the Hubble constant at present time and Ω_m is the matter density parameter. A detailed presentation of this algorithm can be found in (Forero-Romero et al. 2009).

The second tensor is the velocity shear:

$$\Sigma_{\alpha\beta} = -\frac{1}{2H_0}\left(\frac{\partial v_\alpha}{\partial r_\beta} + \frac{\partial v_\beta}{\partial r_\alpha}\right), \qquad (4)$$

where v_α correspond to the components of the peculiar co-moving velocities. With this definition the trace of the shear tensor is minus the divergence of the velocity field normalized by the Hubble constant $-\nabla\cdot v/H_0$. A detailed description of this algorithm can be found in (Hoffman et al. 2012).

4.1 Numerical considerations

In this paper we compute the cosmic web on cubic grids of two different resolutions 256^3 and 512^3. For the T-Web we interpolate first the matter density field using a Cloud-In-Cell (CIC) scheme. Then we smooth using a Gaussian kernel with a spatial variance equal to the size of one grid cell. This smoothed matter density field is transformed into Fourier space to solve the Poisson equation and find the gravitational potential ϕ. The Hessian is computed a finite differences method. Finally, the eigenvalues and eigenvectors are computed on each grid point.

For the V-Web we interpolate first the momentum density field over a grid using the CIC scheme and then apply a gaussian smoothing with a spatial variance of one grid cell. We use the matter density field, which is also CIC interpolated and gaussian smoothed, to normalize the momentum field. This ratio between the momentum and matter density field is what we consider as the velocity field to compute the shear tensor on each grid point. In this case we also compute the eigenvalues and eigenvectors on each grid point.

5 OUR NUMERICAL EXPERIMENTS

In this paper we use the data and the methods described above to perform three diferent kinds of measurements.

5.1 Preferential Alignment

The first measurement is a rough approximation to find out along which axes are halos aligned. We call this Preferential Alignment (PA).

We use the fact that for a given vector under study $\hat{a}$ and the tree eigenvectors the following identity holds

$$(\hat{s}\cdot\hat{e}_1)^2 + (\hat{s}\cdot\hat{e}_2)^2 + (\hat{s}\cdot\hat{e}_3)^2 = 1. \qquad (5)$$

Using this we know that all halos can be splitted into three groups:

(i) Halos with $(\hat{s}\cdot\hat{e}_1)^2 > (\hat{s}\cdot\hat{e}_2)^2$ and $(\hat{s}\cdot\hat{e}_1)^2 > (\hat{s}\cdot\hat{e}_2)$, which can be considered to aligned mostly along $\hat{e}_1$.

(ii) Halos with $(\hat{s}\cdot\hat{e}_2)^2 > (\hat{s}\cdot\hat{e}_2)^2$ and $(\hat{s}\cdot\hat{e}_2)^2 > (\hat{s}\cdot\hat{e}_3)^2$, which can be considered to aligned mostly along $\hat{e}_2$.

(iii) Halos with $(\hat{s}\cdot\hat{e}_3)^2 > (\hat{s}\cdot\hat{e}_1)^2$ and $(\hat{s}\cdot\hat{e}_3)^2 > (\hat{s}\cdot\hat{e}_1)^2$, which can be considered to aligned mostly along $\hat{e}_2$.

If the halo population does not show any preferential alignment, then all the halos must be evenly distributed along these three populations. On the contrary, if there is more than one third of the halo population in one of these sets, then we can talk about a preferential alignment along one of the axis. However, this statistic does not give a precise answer on the degree of the alignment

5.2 Average Alignment Angle

We emphasize that all the quantities that we compute in this paper are independent of any threshold on the eigenvalues that could be used to make a web clasification into web types. Instead, we focus on the alignments with respect to the eigenvectors regardless of the web type. In this context we recall that the eigenvector $\hat{e}_1$ is vector perpendicular to the plane defining a sheet and also a filamente and that $\hat{e}_3$ is the vector that marks the direction of a filament and lies on the plane of a sheet. Therefore we focus on quantifying the degree of alignment along these two eigenvectors.

This experiment complements the results obtained by the PA satistic by computing the average and standard deviation of $|\langle\hat{s}\cdot\hat{e}_1\rangle|$ and $|\langle\hat{s}\cdot\hat{e}_3\rangle|$. We perform this tests in differet populations split into different mass bins logarithmically spaced between $1\times10^9 h^{-1}\mathrm{M}_\odot$ and $1\times10^{14} h^{-1}\mathrm{M}_\odot$.

In a separate test we make the same measurements but this time splitting the halo sample by other properties such as: circularity, concentration, local matter density, spin and triaxiality. In this case we take the upper and lower 30% of the halos according to each property and measure the strenght of the alignment by the average value of $|\langle\hat{s}\cdot\hat{e}_1\rangle|$ and $|\langle\hat{s}\cdot\hat{e}_3\rangle|$.

6 RESULTS

6.1 Preferential Alignment

Figure 1 presents all the results for the preferential alignment (PA) summarizing to a good extent the main results of this paper.

For shape alignment and the Tweb (upper row, right column) we find a strong preferential alignment along the third eigenvector $\vec{e}_3$. This signal incresases steadily with mass and is almost independent of the grid resolution. At high masses between 70% and 100% of the halos have their major axis aligned along $\vec{e}_3$ which means that they mostly lie along filaments and sheets.

The shape alignment and the Vweb (upper row, left column) gives a different perspective. Firstly, there seems to be little evidence for an alignment for masses below $10^{11} - 10^{12} h^{-1}\mathrm{M}_\odot$, depending on the grid resolution. Secondly, the alignment at higher masses goes along the first eigenvector $\vec{e}_1$ meaning that they mostly lie perpendicular to the filaments and sheets. In the discussion section we clarify this result that at first might seem puzzling.

For fhe angular momentum alignment and the Tweb (middle row, right column) we find that at low masses
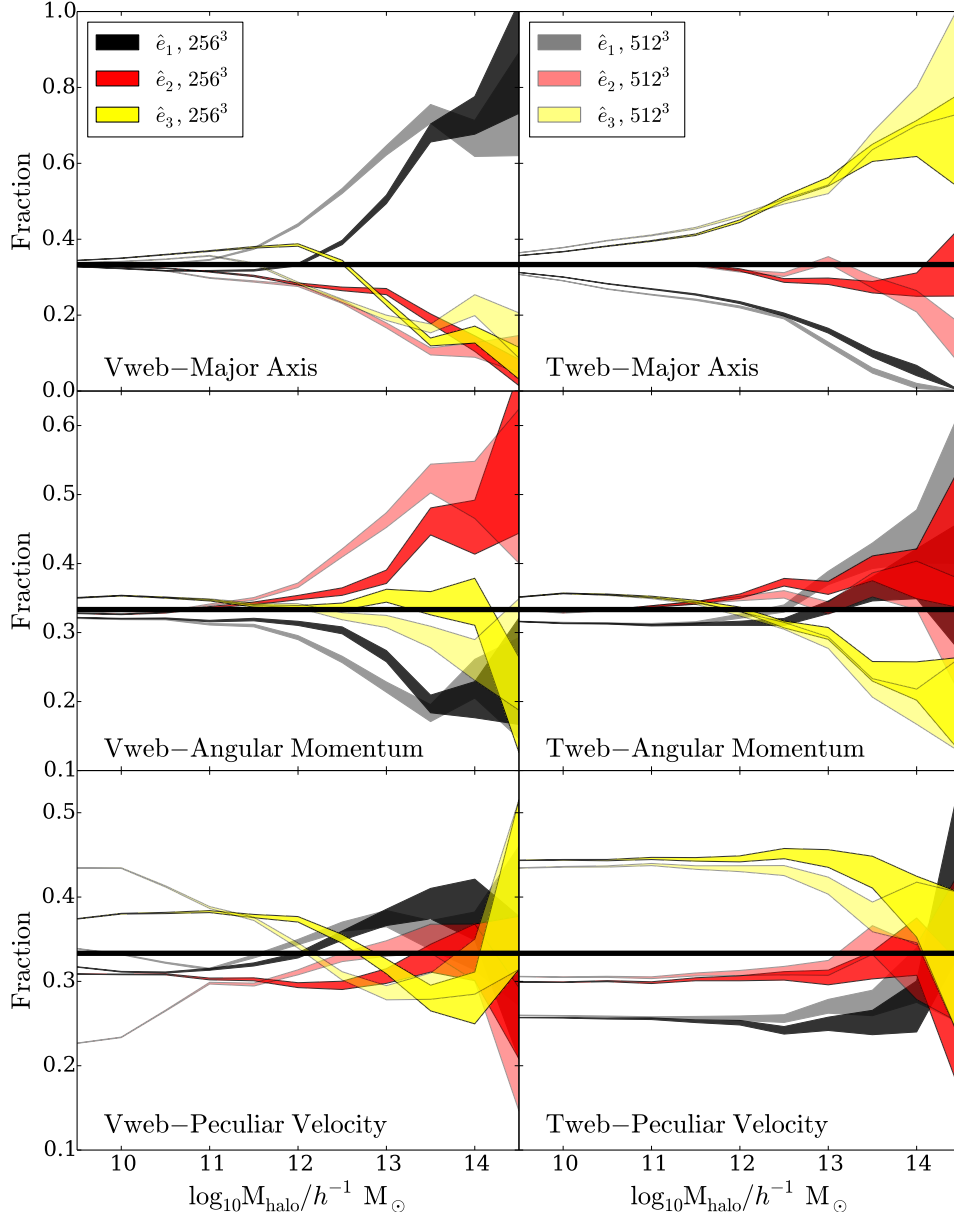
Figure 1. Fraction of halos in a mass bin that show a preferential alignment with respect to an eigenvector. Each row presents on of the three properties studied in this paper: shape (major axis), angular momentum and peculiar velocity. Left column presents the results against the Vweb and the right the Tweb. Strong colors refer to 256^3 grid resolutions and lighter colors to a 512^3 grid. The thick black horizontal line at 0.33 corresponds to the expected fraction for a random vector field.

$< 10^{12}h^{-1}M_\odot$ no evidence for any alignment. At higher masses $> 10^{12}h^{-1}M_\odot$ there is weak signal of preferential alignment along the first and second eigenvectors, between 35% to 45% of the halos are aligned with respect to $\vec{e}_1$ and $\vec{e}_2$. Correspondingly, between 10% to 20% of the halos are aligned along respect to $\vec{e}_3$. This means that most of the halos are perpendicular to the filaments and do not have a clear alignment with respect to walls.

The angular momentum in the Vweb (middle row, left column) presents a a signal of alignment along the second eigenvector $\hat{e}_2$, between 45% to 60% of the halos are aligned along that direction. While there is a minority of halos aligned with $\vec{e}_1$. There a clear change in trends around $10^{11}h^{-1}M_\odot$-$10^{12}h^{-1}M_\odot$ depending on the grid resolution;

below that mass range there is no evidence for alignment while at higher masses appear all the trends we describe. This means that most of the halos tend to lie along walls but do not have a clear alignment with respect to filaments.

The peculiar velocities show a weak but consistent alignment along the third eigenvector $\vec{e}_3$ of the Tweb for all masses below $10^{13.0}h^{-1}M_\odot$-$10^{13.5}h^{-1}M_\odot$ depending on the grid resolution. 45% of the halos are aligned while only 25% are aligned along the first eigenvector $\vec{e}_1$. This suggests that halos tend to move along filaments and parallel to the walls, except at higher masses where the alignments get randomized. In contrast, the peculiar velocities with respect to the Vweb do not show any clear alignment trend.

In the next subsections we present a complementary ac-

count of this results by presenting quantitative results of the average angle between vector pairs describing the alignments discussed so far.

6.2   Shape Alignment

Figure 2 presents the main results for the angles between the first and third eigenvectors and the major shape axis as a function of halo mass.

In the case of the Vweb (left column) we have a clear alignment with respect to the first eigenvector at high masses $> 10^{12}h^{-1}\mathrm{M}_\odot$, with values $|\langle\cos\theta\rangle| \approx 0.8$ well above the expected value of 0.5 for random distribution. With respect to the third eigenvector we measure an anti-alignment with $|\langle\cos\theta\rangle| \approx 0.3$. For low masses $< 10^{12}h^{-1}\mathrm{M}_\odot$ we do not detect any aligmnent signal. This is consistent with the PA results of massive halos perpendicular to filaments and parallel to walls.

The Tweb (right column) show alignment trends starting at masses of $10^{10}h^{-1}\mathrm{M}_\odot$, two orders of magnitude less than the V-web. In this case we measure an alignment along the third eigenvectors and an antialignment along the first eigenvector. In the later case at the highest masses $|\langle\cos\theta\rangle| \approx 0.8$ while in the former $|\langle\cos\theta\rangle| \approx 0.2$. This strong alignment/antialignment signal mirrors the interpretation from the PA results that describe halos lying parallel both to filaments and walls.

6.3   Angular Momentum Alignment

We now take a look at the angular momentum alignment. Figure 3 shows the results as a function of halo mass following the same panel distributio as in Figure 2. In all cases we see that these alignment trends are weaker than shape alignments. For the Vweb low mass halos $< 10^{12}h^{-1}\mathrm{M}_\odot$ do not show any preferential alignment with the cosmic web. Halos more massive than this threshold have their angular momentum slightly perpendicular to the direction defined by the first eigenvector and uncorrelated to the third eigenvector. This translates into a weak tendency for the angular momentum to lie parallel to walls.

In the case of the Tweb, the alignment for low mass halos $< 10^{12}h^{-1}\mathrm{M}_\odot$ is also absent. More massive halos present a weak alignment along first eigen vector and anti-alignment with the third eigenvector. This provides a quantitative expression of the results derived from the preferential alignment whereby the angular momentum is weakly perpendicular to filaments.

6.4   Peculiar velocity Alignment

Possible conclusion. Prolateness follow concentration. In the Tweb Angular momentum alignment is influenced by spin at higher masses. In the Vweb angular momentum alginment is influenced by all factors. In the peculiar velocity alginment only spin seemss to have an effect.

6.5   What drives the alignment

We wish to understand what other selection criteria on halo properties can produce a stronger local alignment for the shape, spin and peculiar velocities. We split the halo population into low and high mass halos imposing a cut at $M_{\mathrm{halo}} = 10^{11}h^{-1}\mathrm{M}_\odot$. This allows us to have robust statistics on the high mass end. We have also computed these results for a cut at $M_{\mathrm{halo}} = 10^{12}h^{-1}\mathrm{M}_\odot$ and checked that the results we report below are not affected by this change.

For each mass interval we perform cuts in the following properties: spin, concentration, triaxiallity, circularity and density. We measure the web alignments in two sets, each one including the 30% of halos in the lower/higher end of the corresponding property.

7   DISCUSSION

We do not find a strong signal for the alignment of spin and the cosmic web. A significant correlation signal has been recently measured between the spin and the cosmic vorticity (**?**Laigle et al. 2013). This two facts are consistent with spin being produced by the non-symmetric part of the shear and tidal tensors.

7.1   Interweb Alignment

In the first place we wish to directly compare the results of the two algorithms. For the two algorithms we have the information for the eigenvectors and the eigenvalues on exactly the same positions defined by the grids. This allows us to-compute the pair-wise alignment between the eigenvectors in the two web finders.

We are mainly interested in the alginment of the web with the halos. Therefore we restrict our analysis to the grid cells that are occupied by halos. If we had decided to perform this kind of analysis on all the grid cells, the statistics would be dominated by the void regions, because the dominate in number the fraction of cells in the simuation.

Figure 6 shows the results of the inter-web alignment as a function of halo mass. It clearly stands out that the eigenvectors are aligned for low mass halos but are close perpendicular to each other at the location of the most massive halos. There is a transition scale around $(10^{11.5} - 10^{12.5})h^{-1}\mathrm{M}_\odot$ depending on the grid resolution. The coarse grid (256^3) shows the transition at higher masses than the fine grid (512^3).

For both resolutions, the halos more massiven than $10^{13}h^{-1}\mathrm{M}_\odot$ are locate in regions where the fastest momentum-weighted collapse direction (defined by the V-web) is perpendicular to the direction where the tidal compression is the highest.

The fact that this trend is less evident at low resolution and low masses, hints that the flip is actually related to the overdensity values, i.e. to the degree of non-linearity, in the corresponding spatial scales.

8   CONCLUSIONS

We have examined the alignment of shape, angular momentum and peculiar velocity of dark matter halos with respect to the cosmic web. We use publicly available data from two algorithms implemented on a large cosmological N-body simulation to study halo populations spanning five orders of
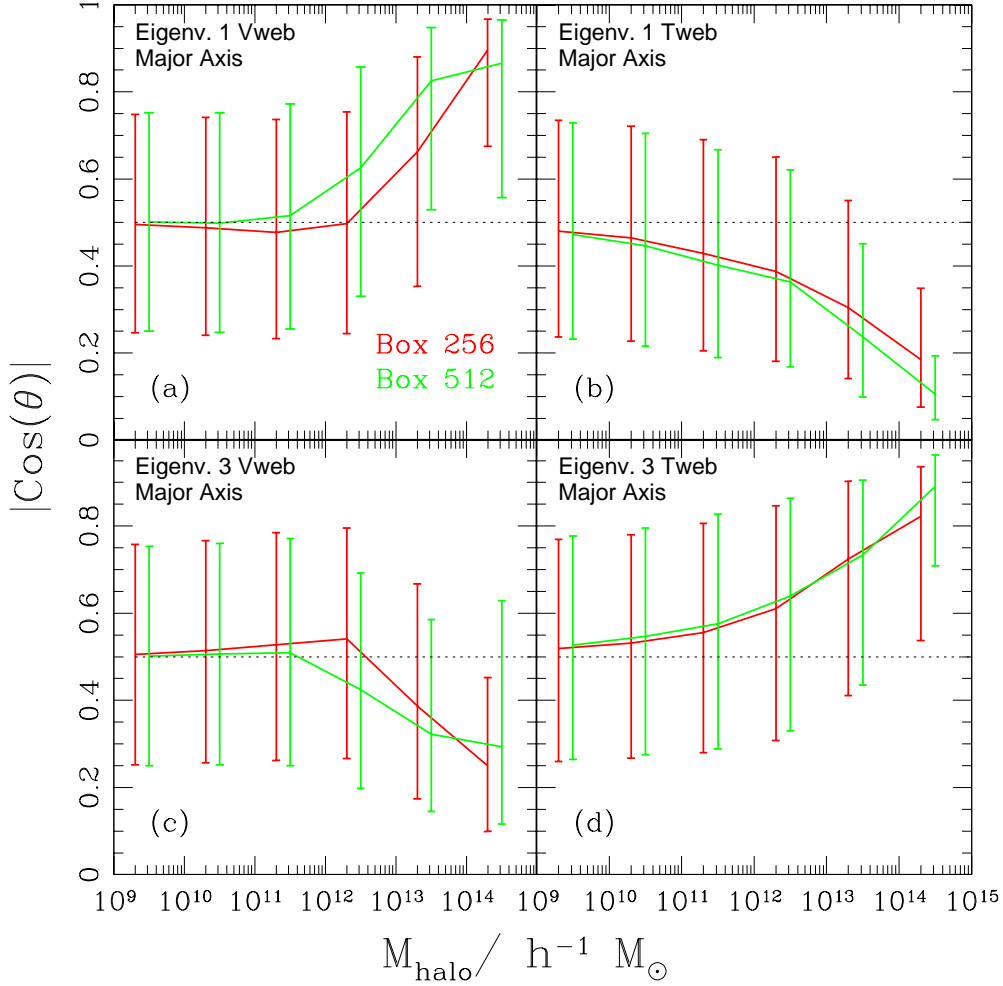
Figure 2. Median of $\cos\theta$ quantifying the shape alignment for the Vweb (left) and the Tweb (right) at two different grid resolutions. In the upper (lower) panels the angle θ is measured between the halo major axis and the first (third) eigenvector.

magnitude in mass. The first algorithm uses the tidal field and the second the velocity shear, both present local results on scales of $0.5h^{-1}$Mpc to $1.0h^{-1}$Mpc .

APPENDIX A. DETAILED DESCRIPTION OF PREVIOUS THEORETICAL RESULTS

The tidal connection between voids in simulations (Platen et al. 2008), the alignment of observed galaxies with the inferred tidal field(Lee & Erdogdu 2007; Jones et al. 2010). There are other kind of alignment statistics based on modifications of the correlation (Paz et al. 2008; Faltenbacher et al. 2009) that go beyond a local computation and therefore are not reviewed in detail in this paper.

- (Libeskind et al. 2013) Studies shape and spin alignment with the cosmic web defined by the velocity shear tensor method described in this paper.

The simulation has 2048^3 particles in a box of $250h^{-1}$Mpc , corresponding to a particles mass of $1.3\times10^8 h^{-1}$M$_\odot$. Halos

are found using a FOF halo finder with $b = 0.17$. The catalog only include halos more massiven than $3 \times 10^9 h^{-1}$M$_\odot$.

The shape is defined from the reduced inertia tensor. Results are reported for three mass bins $M_{\rm vir} < 10^{11.5} h^{-1}M_\odot$, $11^{11.5} < M_{\rm vir} < 12^{12.5} h^{-1}M_\odot$ and $M_{\rm vir} > 12^{12.5} h^{-1}M_\odot$.

The identification of the cosmic web is done on a grid of 256^3 with a gaussian smoothing of $\sim 1h^{-1}$Mpc over the velocity field. We define this velocity field as the ratio of a momentum density to the matter density field. The details of this approach are described in the Appendix .

The aligmnet signal of the spin is very weak while the shape alignment signal is very strong. The shape alignment is such that the eigenvector corresponding to the smallest eigenvalue is aligned with the major axis. This effect is stronger for more massive halos. In other words the major axis of a halo is aligned with a filament, and lies on the plane that define a sheet. However the spin is antialigned with the filament for massive halos and weakly aligned for low mass halos.

- (Trowland et al. 2013)

The simulation is the millennium run, which has 2160^3 particles in a volume of $500h^{-1}$Mpc on a side. This corresponds to a particle mass of $8.6 \times 10^8 h^{-1}$M$_\odot$. The cata-
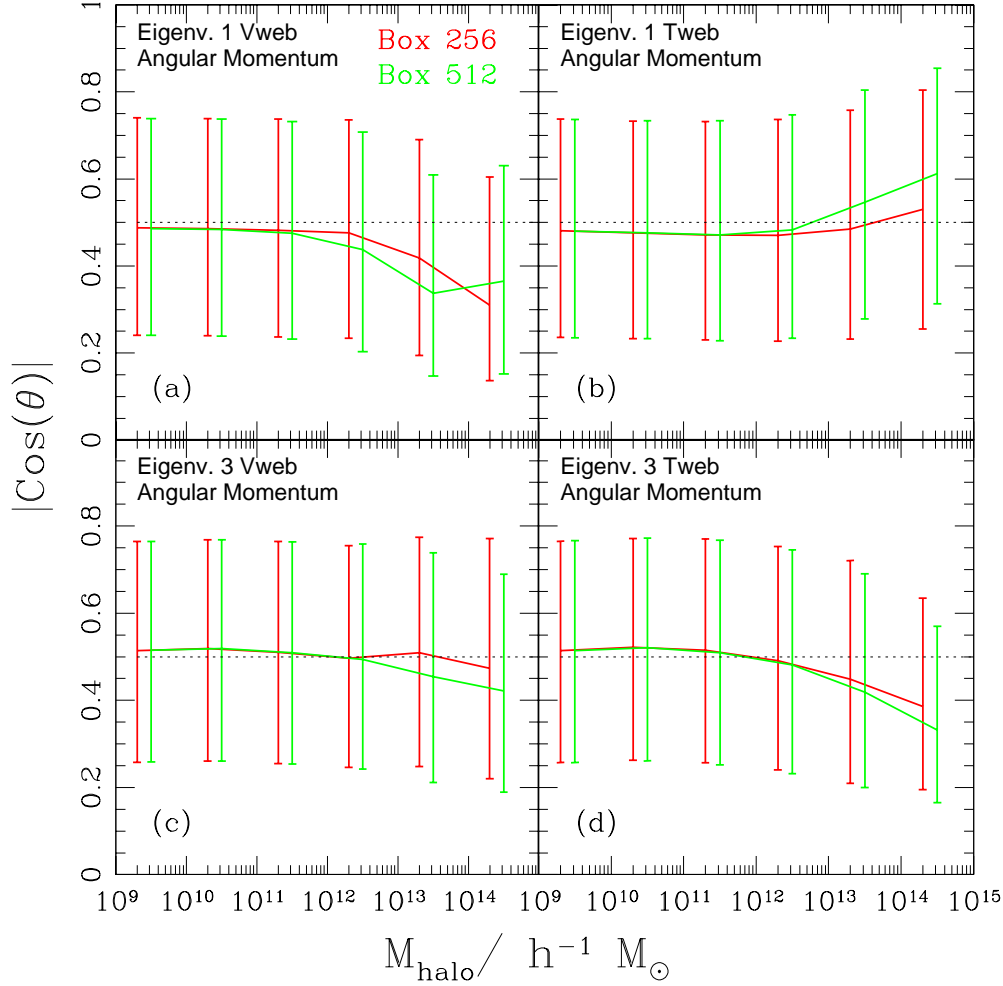
Figure 3. Median of $|\cos\theta|$ quantifying the angular momentum alingment for the Vweb (left) and the Tweb (right) for two different grid resolutions. In the upper (lower) panels the angle θ is measured between the first (third) eivenvector and the angular momentum vector.

log uses both halos and subhalos which were identified with SUBFIND. Only halos with more than 500 particles were kept to get a robust computation for the spin. For each halo the spin is defined as the sum of the angular momentum of each particle with respect to the center of mass.

The method to define the filamentary structure is based on the eigenvalues of the hessian of the density.However the analysis are reported ona box of $300h^{-1}$Mpc on a side. Four different gaussian smoothing scales are used: 2.0, 3.0 and $5.0h^{-1}$Mpc .

The authors report a slight alignment signal of spin against the principal filament axis. By fitting the following functional form to the $\cos(\theta)$ distribution

$$P(\cos\theta) = (1-c)\sqrt{1+\frac{c}{2}}\left[1-c\left(1-\frac{3}{2}\cos^2\theta\right)\right]^{-3/2}, \quad (6)$$

they are able to quantify the degree of alignment ($c < 0$) or antialignment ($c > 0$). This parameterization is based on theoretical expectactions of Tidal Torque Theory (TTT) (Lee et al. 2005). At $z = 0$, the reported value is $c =$

0.035 ± 0.004, where the uncertainty was calculated using bootstraping and resampling.

When the halo sample is divided between low mass and high mass halos with a transition scale $M_\star = 5.9 \times 10^{12} M_\odot$, there is an anti-alignment above this mass and an alignment below it.

• (Codis et al. 2012) Studies the alignment of the spin of dark matter halos relative to the surrounding large scale structure and to the tidal tensor eigenvalues.

They use a dark matter simulation with 4096^3 DM particles in a cubic periodic box of $2000h^{-1}$Mpc on a side, which corresponds to a particle mass of $7.7 \times 10^9 M_\odot$. Halos are identified using a FoF algorithm with a linking legth of 0.2 keeping all halos with more than 40 particles, which sets the minimum halo mass to be $3 \times 10^{11} M_\odot$. In their work the particles were sampled on a 2048^3 grid and the density field was smoothed with a gaussian fileter over a scale of $5h^{-1}$Mpc corresponding to a mass of 1.9×10^{14}. The skeleton was computed over 6^3 overlapping subcubes and then reconnected.

The filament finder algorithm is based on Morse theory and defines a Skeleton to be the set of critical lines join-
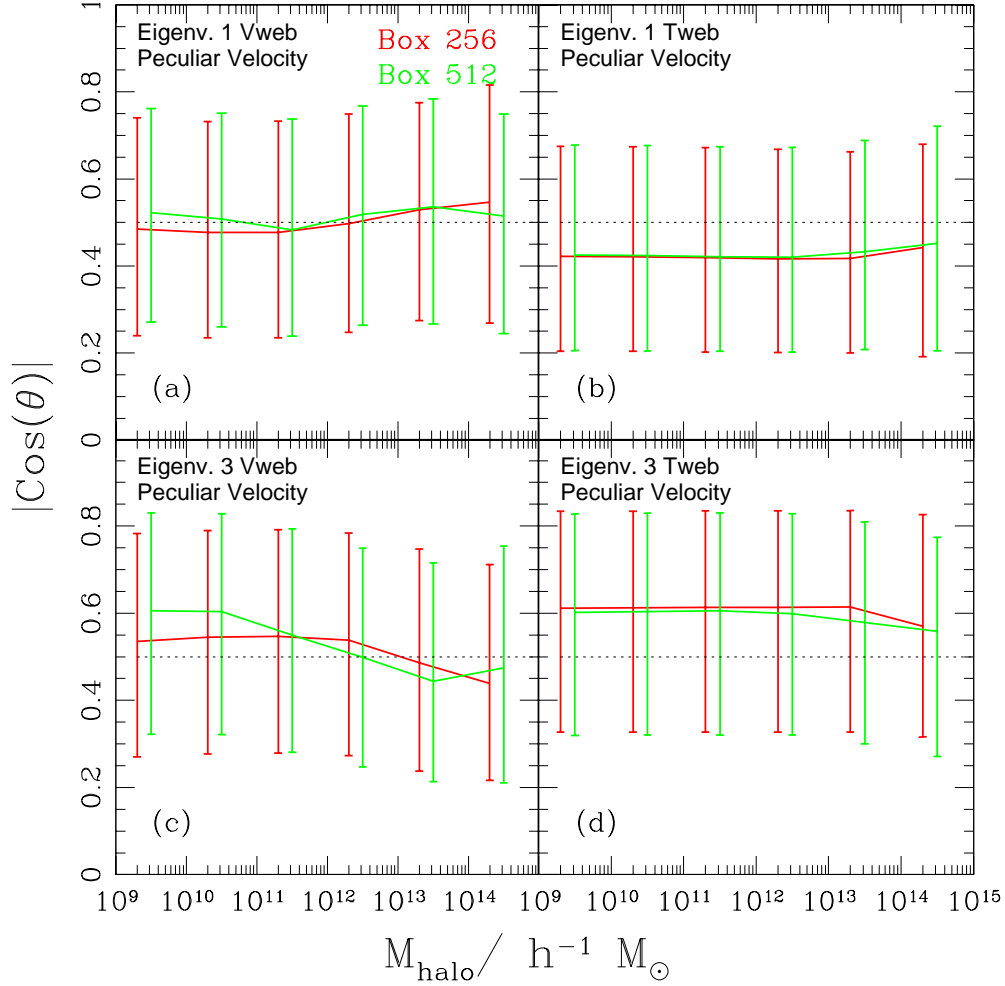
Figure 4. Median of $\cos\theta$ quantifying the peculiar velocity alignment with the Vweb (left) and the Tweb (right) at two different grid resolutions. In the upper (lower) panels the angle θ is measured between the first (third) eivenvector and a halo's peculiar velocity.

ing the maxima of the densit field through saddle points following the gradient. They also compute the hessinan of the potential over the smoothed density field to get their eigenvectors.

The spin of the halo is defined as $m_p \sum_i (r_i - \bar{r}) \times (v_i - \bar{v})$ where $\bar{r}$ is the center of mass of the halo and $\bar{v}$ is the average velocity.

They measure the sping alignment with each one of the eigenvectors. With repecto to the minor eigenvector e_1 there is antialignement for masses $M > 5 \times 10^{12} \mathrm{M}_\odot$ and alignment for masses $< 5 \times 10^{12} \mathrm{M}_\odot$. With respect to the intermediate eigenvector e_2 there is a strong alignment at high masses and no alignment for low masses, with respecto the major eigenvector e_3 there is an anti-alignment signal at all masses. The results from the Skeleton algorithm are in perfect agreement with the results from the Tidal web. The transitional mass is weakly dependent on the smoothing scale, varing between $1 - 5 \times 10^{12} h^{-1} \mathrm{M}_\odot$ for smoothing scales between $1.0 - 5.0 h^{-1}\mathrm{Mpc}$.

• (Zhang et al. 2009) Study the spin and shape alignment against filaments.

They use a dark matter simulation with 1024^3 DM particles in a periodic box of $100\ h^{-1}\mathrm{Mpc}$ on a side. The particle mass is $6.92 \times 10^7 h^{-1}\mathrm{M}_\odot$. Dark matter haloes are found using a FOF algorithm with a linking length of 0.2 times the interparticle distance. Only halos with more than 500 particles are retained for further analysis.

The angular momentum is measured with positions repect to the center of mass and the shape is determined using the non-normalized moment of inertia tensor.

The environment is found using the hessian of the density. The density field was interpolated over a 1024^3 grid and then smoothed with a Gaussian filter of scale $R_s = 2.1 h^{-1}\mathrm{Mpc}$. There are two methods to define the direction of a filament. The first method uses the eigenvalues of the hessian density, howevere they define the filament direction with the eigenvector corresponding the single positive eigenvalue of the hessian. The second method used a line that connects the two terminal halos in a filament segment.

The characterization of the alingment with the $\cos(\theta)$ statistic. For the method that uses the eigenvectors, they find that the strenght of the spin alignment decreases with halo mass. For the shape they study the alingment of the major axis with the filament. The find an alignment signal in all mass bins, with an stronger effect for more massive halos.
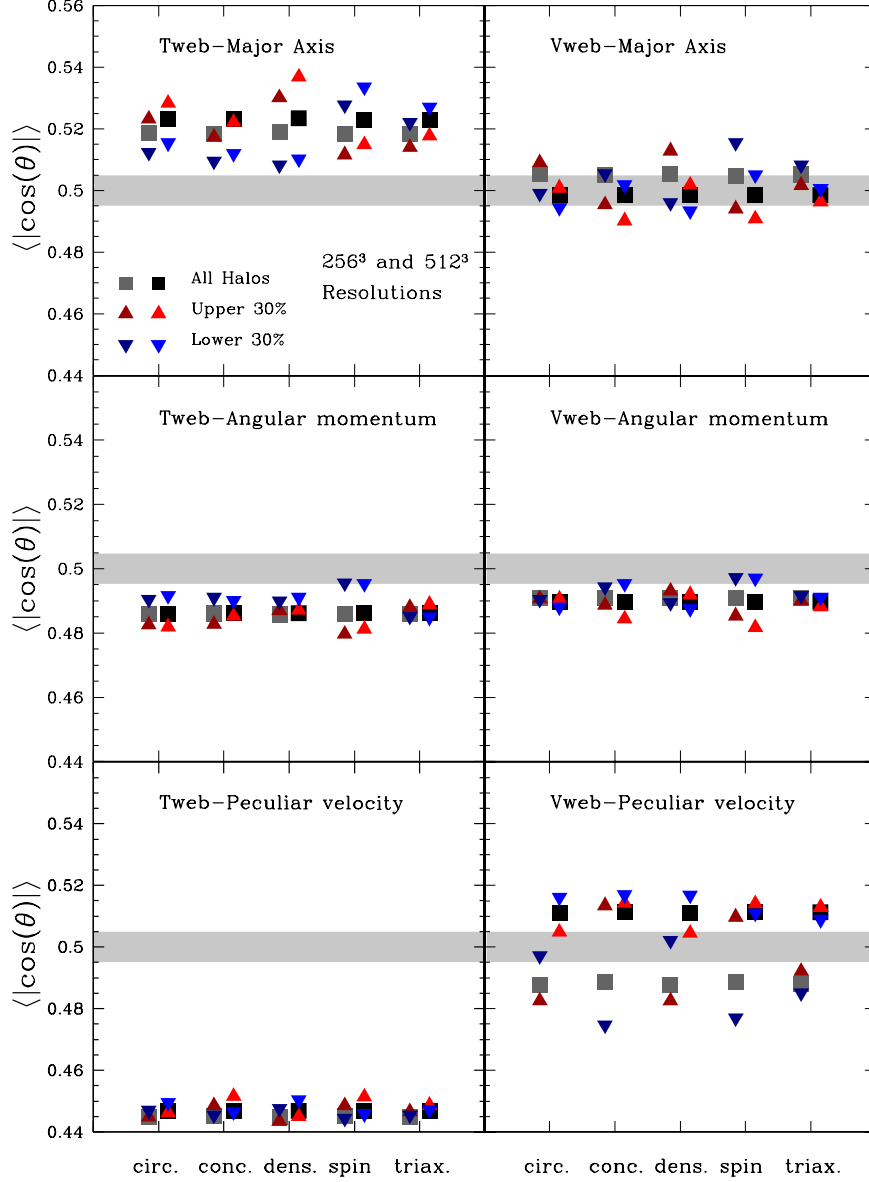
Figure 5. The alignment is always taken with respect to the first eigenvector.

In a final experiment they measure the spin alignment in four different samples that separated by the strength of the shape alignment. They find that halos anticorrelated in shape, show a strong sping correlation going to the extreme where there is a strong spin anticorrelation for halos with a strong shape correlation. This means that the halos with strong spin alignment are not the same halos showing strong shape alignment.

• (Aragón-Calvo et al. 2007) The method is the Multi-scale Morphology Filter which is based on the Hessian matrix of the density field, where the density field is computed from the particle distribution using a Delaunay tesselation field estimatior (DTFE), which is self-adaptive. This allows them to identify clusters, filaments and walls.

The simulation has 512^3 particles in a cubic box of $150h^{-1}$Mpc . The mass per particle is $2 \times 10^9 h^{-1}$M$_\odot$. Halo identitification is done with the HOP algorithm. They keep

halos with more than 50 partices and less than 5000, defining a mass range of $1 - 100 \times 10^{11} h^{-1}M_\odot$.

The principal axes of each halo are computed from the non-normalized inertia tensor. The inertian tensor and the angular momentum are computed with respect to the center of mass of the halo.

They compute two angles, one with respect to the direction defining the filaments and the other the walls. Their results make a distinction between halos of more massive and less massive than $10^{12} h^{-1}$M$_\odot$.

The halo spins tend to lie on the plane of the wall. This is stronger for massive halos.The effect for filaments is weaker: low mass halos tend to lieparallel to their host filament, while high mass halos tend to be perpendicular.

Theres is a very strong effect for the principal axes of halos in filaments to be strongly correlated with the direction of
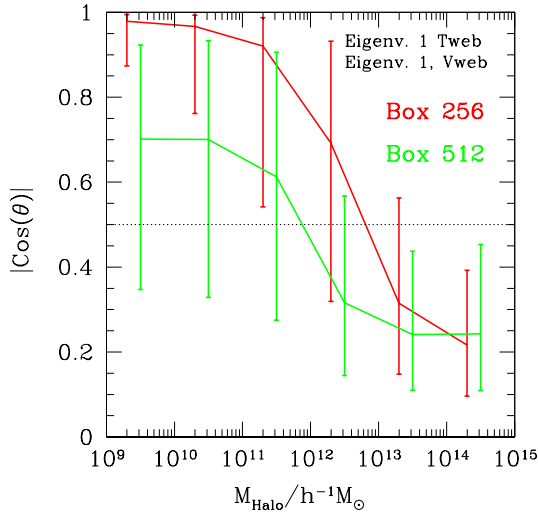
Figure 6. Median of the interweb alignment for the two grid resolutions as a function of the dark matter mass corresponding to the halos where the measurement was made. The error bars indicate the lower and upper quartiles (Figure in color in the web version).

the filaments. The minor axis tend to be perpendicular to the filament. This effect is stronger for larger halos.

The effect in walls is less strong ,but still the minor axis tend to lie perpendicular to the wall, while the other axis then to lie over the wall. The effect is stronger for massive halos.

They find that spins and shapes of dark matter halos are significantly correlated with each other and with the orientation of their host structures.

• (Hahn et al. 2007)The method is the Tweb. They use three simulations each of 512^3 particles, with sizes $L_1 = 45h^{-1}\text{Mpc}$, $L_2 = 90h^{-1}\text{Mpc}$ and $L_3 = 180h^{-1}\text{Mpc}$, this corresponds to particle masses of $4.7, 38.0, 300 \times 10^7 h^{-1}\text{M}_\odot$. The normalization is $\sigma_8 = 0.9$. Halo identification was done with a FOF algorithm with 0.2 times the interparticle distance. They consider halos of at least 300 particles.

The web is obtained for a grid of 1024^3 cells, the density field is obtained with a CIC interpolation and smoothed using a Gaussian Kernel. In the rest of the paper all the results correspond to a smoothing scale of $R_s = 2.1h^{-1}\text{Mpc}$.

They Report on the angle between the halo angular momentum vector and the eigenvector corresponding to perpendicular directions to the sheets and the direction of the filaments. This is divided in two halo populations: $5 \times 10^{10} - 1.0 \times 10^{12}$ and $> 10^{12}$. There is a weak antialignment in the case of the filaments and a stronger antialignment in the case of the sheets. For the sheets the effect is stronger for the massive bin. In the filaments the alignment is weak regardless of the mass. They do not report any other significan statistic, but recognize that they suffer from small-number statistics in voids).

They do not see any strong dependance of the environment in the shape. They do not measure the shape alinment.

• (Brunino et al. 2007) Uses a DM only N-body simulation (the Millennium Run) to study the shape and angu-

lar momentum alignment with respect to large cosmological voids.

The voids are found with a spherical void finder. This algorithm first looks for potential void centers in the underdense regions of the simulation. These positions define the centers of spheres that are empty of halos above a given mass threshold. Only voids with radius larger than $10h^{-1}\text{Mpc}$ were considered for further analysis.

Halos were identified by linking particles with density exceeding 900 times the background density in order to keep the analysis of shape and angular momentum on the core of the halo. Only halos with masses in the range $8.6 \times 10^{11} h^{-1}\text{M}_\odot < M_\text{h} < 8.6 \times 10^{12} h^{-1}\text{M}_\odot$ were included analized to measure their angular momentum and the inertia tensor, both in a non-normalized way.

For the purpose of measuring alignments a second cut is imposed whereby only halos within a shell of radius $R_{void} < r < 1.05R_{void}$. The alignment is then measured between the vector connecting the center of the void to the halo in question and the vector of interest.

The results show that there is a strong alignment of halo shape in such a way that the major axis is parallel to the shell surrounding the void. In the case of angular momentum there is not a significant signal for alignment.

• (Basilakos et al. 2006) Use a cosmological SPH+N-body simulation to measure the alignment of cluster halos with their parent supercluster. For both the cluster halos and parent super-cluster they define the shape via the non-normalized inertia tensor. The find that strenght of the alignments increases with the degree of filamentarity of the supercluster.

The simulation has 2×512^3 particles in a box of side $500h^{-1}\text{Mpc}$. The dark matter particle mass is $6.6 \times 10^{10} h^{-1}\text{M}_\odot$while for SPH particles is $1.2 \times 10^{10} h^{-1}\text{M}_\odot$. The halo finding is done with a FOF algorithm with a linking length of 0.17 and keep objects with more than 100 partcles.

• (Lee & Pen 2002)Observational measurement for the alignment of galaxy spin axes with the local tidal shear field. For the measurement of shear, we have used the Point Source Catalog Redshift (PSCz) survey (a complete redshift survey from the IRAS Point Source Catalog) data. This was done down to a radial comoving distance of $\sim 150h^{-1}\text{Mpc}$.

• (Hatton & Ninin 2001) DM matter only simulation. 256^3 particles, $100h^{-1}\text{Mpc}$, particle mass. Look for alignment of angular momentum vectors with neighbohring structures or other massive structures. They match halos using close pair statistics. They do not find any evidence for a statistically significant mutual alignment of halos on any escale.

REFERENCES

Aragón-Calvo M. A., van de Weygaert R., Jones B. J. T., van der Hulst J. M., 2007, ApJL, 655, L5

Basilakos S., Plionis M., Yepes G., Gottlöber S., Turchaninov V., 2006, MNRAS, 365, 539

Brunino R., Trujillo I., Pearce F. R., Thomas P. A., 2007, MNRAS, 375, 184

Codis S., Pichon C., Devriendt J., Slyz A., Pogosyan D., Dubois Y., Sousbie T., 2012, MNRAS, 427, 3320

Dunkley J., Komatsu E., Nolta M. R., Spergel D. N., Larson D., Hinshaw G., Page L., Bennett C. L., Gold B., Jarosik N., Weiland J. L., Halpern M., Hill R. S., Kogut A., Limon M., Meyer S. S., Tucker G. S., Wollack E., Wright E. L., 2009, ApJS, 180, 306

Faltenbacher A., Li C., White S. D. M., Jing Y.-P., Shu-DeMao Wang J., 2009, Research in Astronomy and Astrophysics, 9, 41

Forero-Romero J. E., Hoffman Y., Gottlöber S., Klypin A., Yepes G., 2009, MNRAS, 396, 1815

Hahn O., Carollo C. M., Porciani C., Dekel A., 2007, MN-RAS, 381, 41

Hatton S., Ninin S., 2001, MNRAS, 322, 576

Hinshaw G., Larson D., Komatsu E., Spergel D. N., Bennett C. L., Dunkley J., Nolta M. R., Halpern M., Hill R. S., Odegard N., Page L., Smith K. M., 2013, ApJS, 208, 19

Hoffman Y., Metuki O., Yepes G., Gottlöber S., Forero-Romero J. E., Libeskind N. I., Knebe A., 2012, MNRAS, 425, 2049

Jones B. J. T., van de Weygaert R., Aragón-Calvo M. A., 2010, MNRAS, 408, 897

Klypin A. A., Trujillo-Gomez S., Primack J., 2011, ApJ, 740, 102

Laigle C., Pichon C., Codis S., Dubois Y., le Borgne D., Pogosyan D., Devriendt J., Peirani S., Prunet S., Rouberol S., Slyz A., Sousbie T., 2013, ArXiv e-prints

Lee J., Erdogdu P., 2007, ApJ, 671, 1248

Lee J., Kang X., Jing Y. P., 2005, ApJL, 629, L5

Lee J., Pen U.-L., 2002, ApJL, 567, L111

Libeskind N. I., Hoffman Y., Forero-Romero J., Gottlöber S., Knebe A., Steinmetz M., Klypin A., 2013, MNRAS, 428, 2489

Paz D. J., Stasyszyn F., Padilla N. D., 2008, MNRAS, 389, 1127

Platen E., van de Weygaert R., Jones B. J. T., 2008, MN-RAS, 387, 128

Riebe K., Partl A. M., Enke H., Forero-Romero J., Gottlöber S., Klypin A., Lemson G., Prada F., Primack J. R., Steinmetz M., Turchaninov V., 2013, Astronomische Nachrichten, 334, 691

Trowland H. E., Lewis G. F., Bland-Hawthorn J., 2013, ApJ, 762, 72

Zhang Y., Yang X., Faltenbacher A., Springel V., Lin W., Wang H., 2009, ApJ, 706, 747